IAC-17-A6.5.5

# Laboratory demonstration of space debris removal by a bi-directional helicon plasma thruster

**Kazunori Takahashi[a]*, Christine Charles[b], Rod W. Boswell[c], and Akira Ando[d]**

[a] *Department of Electrical Engineering, Touhoku University, Sendai, 980-8579, Japan,* kazunori@ecei.tohoku.ac.jp
[b] *Space Plasma and Plasma Propulsion Laboratory (SP3), Research School of Physics and Engineering, The Australian National University, Canberra, ACT 2601, Australia,* christine.charles@anu.edu.au
[c] *Space Plasma and Plasma Propulsion Laboratory (SP3), Research School of Physics and Engineering, The Australian National University, Canberra, ACT 2601, Australia,* rod.boswell@anu.edu.au
[d] *Department of Electrical Engineering, Touhoku University, Sendai, 980-8579, Japan,* akira@ecei.tohoku.ac.jp
* Corresponding Author

# Space debris removal

Orbit transfer of debris is essential for the debris removal technology.

Debris catcher technology

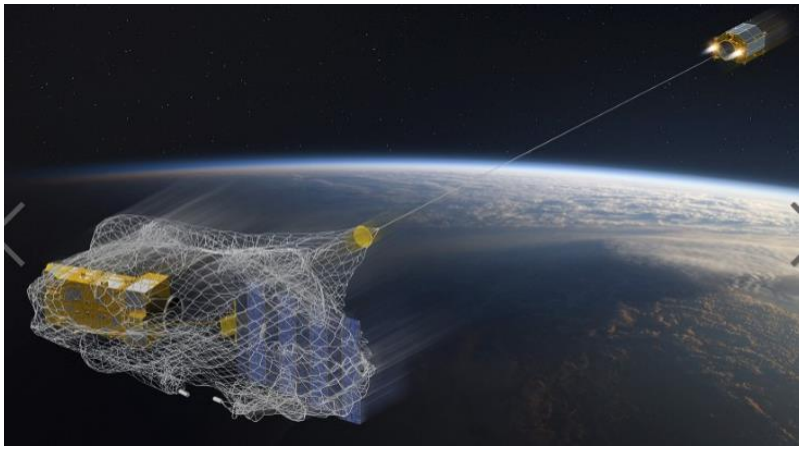

Propulsion device and catcher technology

the ion beam shepherd (IBS) technology

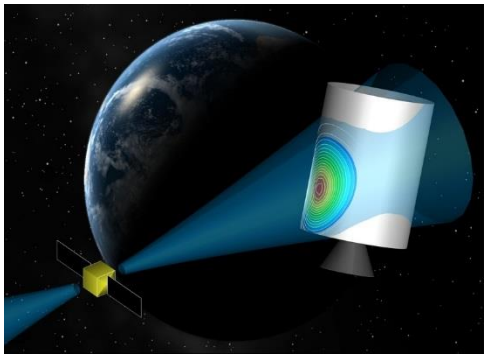

https://leosweep.upm.es/en/

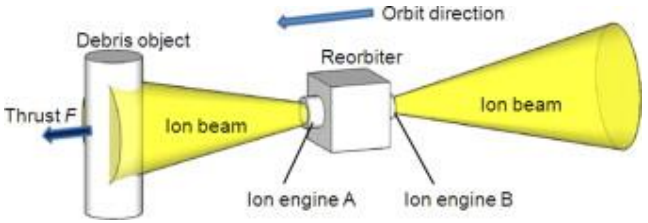


Kitamura et al., Acta Astronautica, 2014

Two propulsion devices (ion thrusters)

# Bi-directional ion acceleration in a helicon source

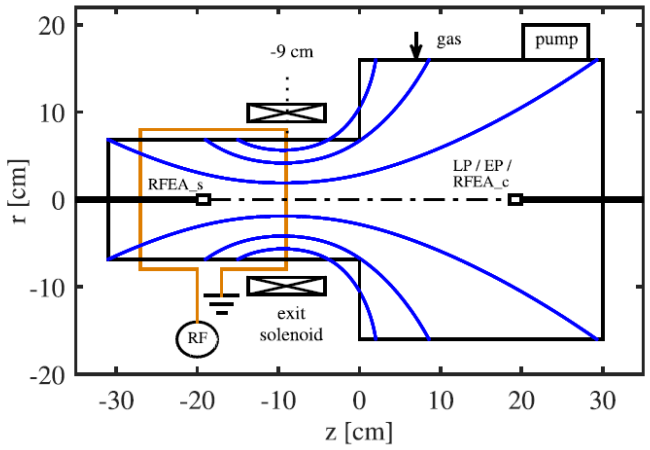


FIG. 1. Chi-Kung reactor implemented with a convergent-divergent magnetic nozzle, showing the major components and diagnostic probes. The calculated field lines are plotted within the reactor geometry.

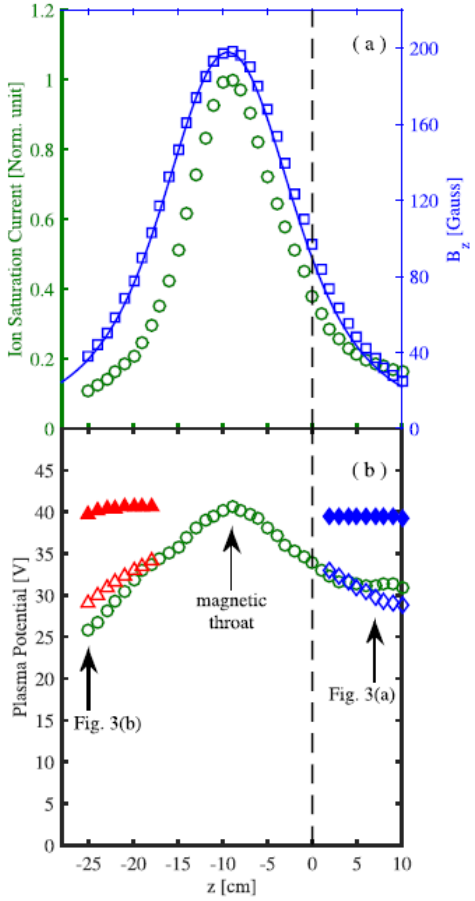


FIG. 2. (a) Right labelled y-axis: On-axis magnetic flux density generated by a current of 9 A supplied into the solenoid, measured using a gaussmeter (◯) and calculated by the Biot-Savart law (solid line). Left labelled y-axis: axial profile of normalized ion saturation current measured by the LP (◯). (b) Axial profiles of plasma potential measured by the EP (◯), beam potential obtained by RFEA_c (◆) and RFEA_s (▲), and plasma potential obtained by RFEA_c (◇) and RFEA_s (△). The vertical dashed line show the location of source-chamber interface at $z = 0$ cm.

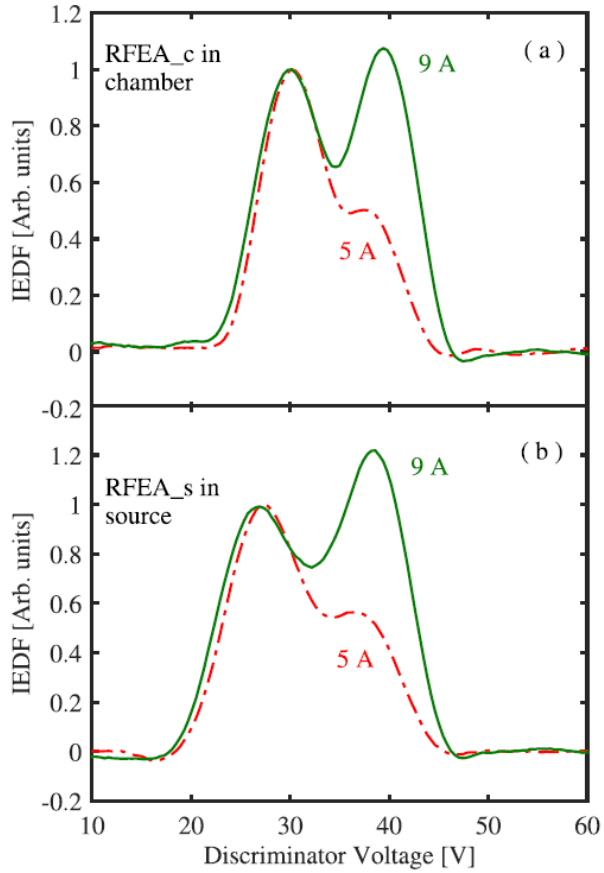


FIG. 3. IEDFs obtained by (a) RFEA_c at $z = 7$ cm in the diffusion chamber and (b) RFEA_s at $z = -25$ cm in the plasma source, for current values of 9A (solid line) and 5A (dashed-dotted line) supplied into the solenoid.

Zhang et al., APL 2016

# Motivation

Demonstrating the space debris removal by one propulsion device (magnetic nozzle helicon thruster).

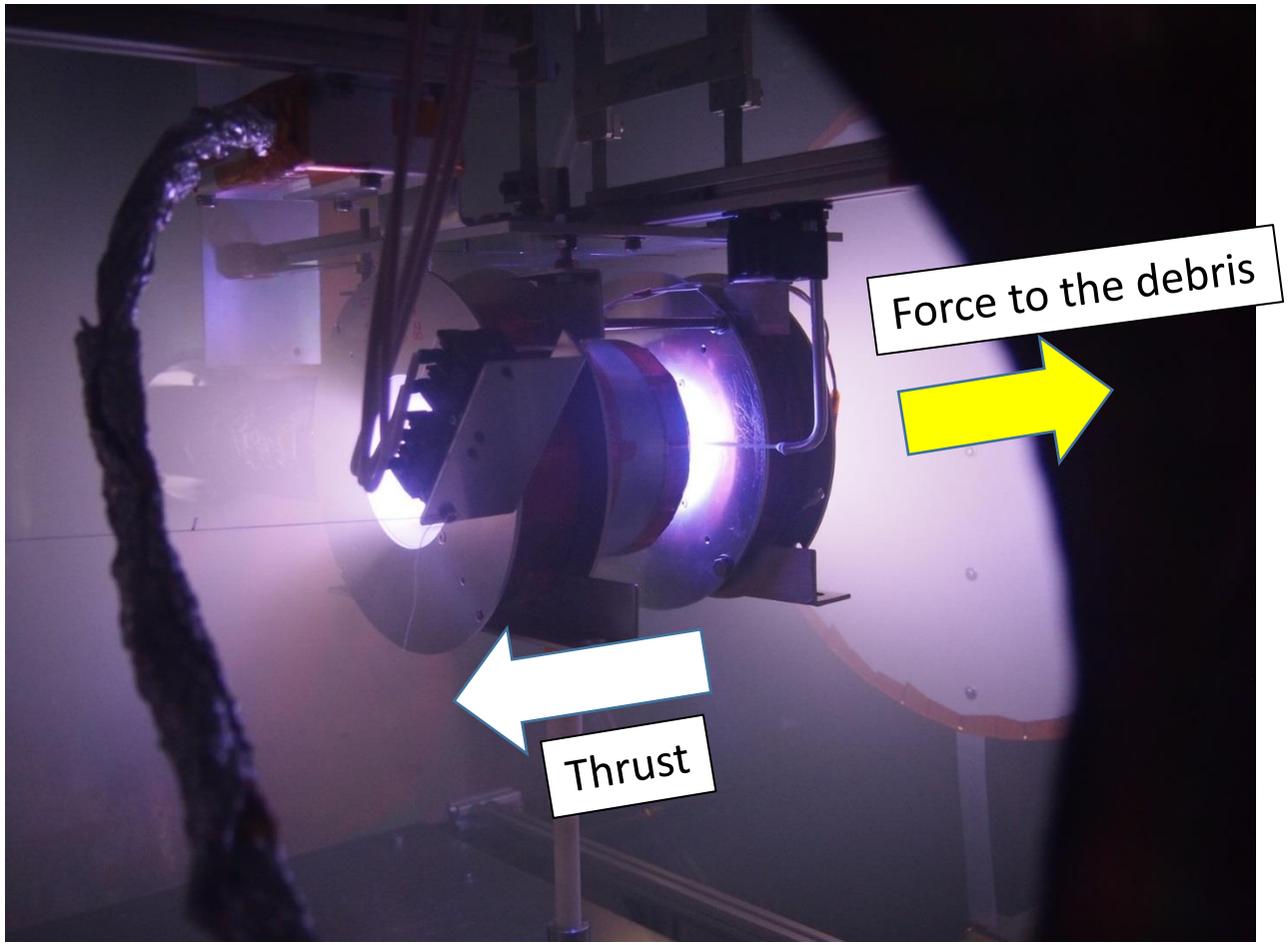

# Thrust generation by the helicon thruster

$$m_j \nabla \cdot (n_j \mathbf{v}_j \mathbf{v}_j) = q_j n_j (\mathbf{E} + \mathbf{v}_j \times \mathbf{B}) - \nabla \cdot \mathbf{P}_j$$

PRL 107, 235001 (2011) PHYSICAL REVIEW LETTERS week ending 2 DECEMBER 2011

**Electron Diamagnetic Effect on Axial Force in an Expanding Plasma: Experiments and Theory**

Kazunori Takahashi,[1,2,*] Trevor Lafleur,[1] Christine Charles,[1] Peter Alexander,[1] and Rod W. Boswell[1]
[1]*Space Plasma, Power and Propulsion Laboratory, Research School of Physics and Engineering, The Australian National University, Canberra ACT 0200, Australia*
[2]*Department of Electrical Engineering and Computer Science, Iwate University, Morioka 020-8551, Japan*
(Received 16 June 2011; published 28 November 2011)

The axial force imparted from a magnetically expanding current-free plasma is directly measured for three different experimental configurations and compared with a two-dimensional fluid theory. The force component solely resulting from the expanding field is directly measured and identified as an axial force produced by the azimuthal current due to an electron diamagnetic drift and the radial component of the magnetic field. The experimentally measured forces are well described by the theory.

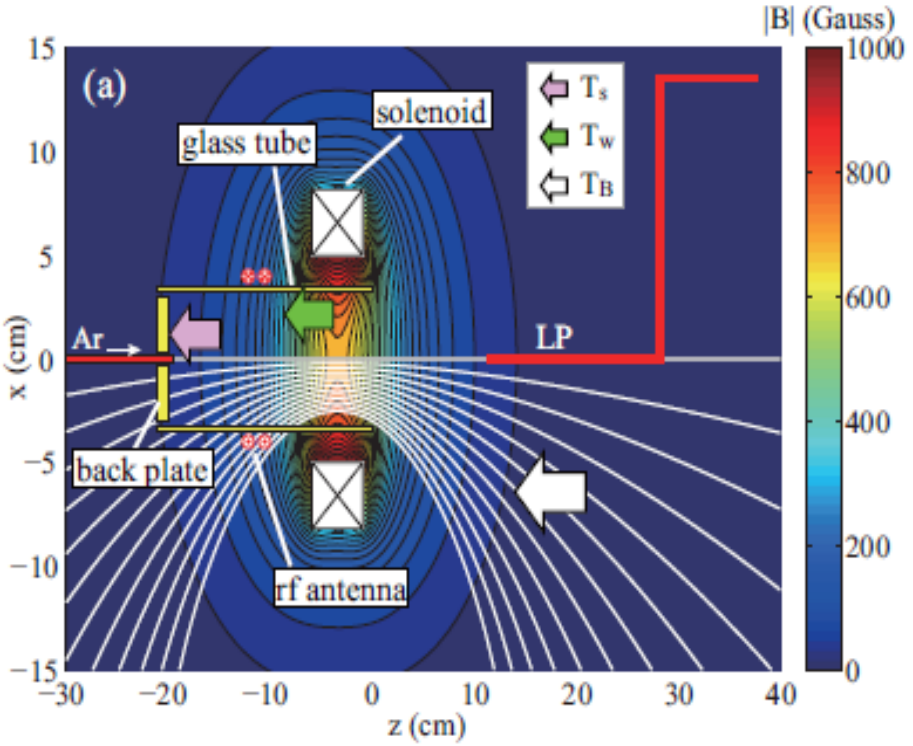


Total momentum (Thrust)

$$T(z) = \iint (p_e + mnu_z^2) d\theta dr$$

$$T_{total}(z) = \boxed{2\pi \int_0^{r_s} r p_e(r, z_0) dr} \quad \boxed{-2\pi \int_{z_0}^{z} \int_0^{r_p(z)} r \frac{B_r}{B_z} \frac{\partial p_e}{\partial r} dr dz} \quad \boxed{-2\pi \int_{z_0}^{z} \int_0^{r_p(z)} \frac{\partial}{\partial r} (rmnu_r u_z)\, dr dz,}$$

$T_s$ $T_B$ $T_w$

# Thrust arising from the MN

PRL **110,** 195003 (2013) PHYSICAL REVIEW LETTERS week ending 10 MAY 2013

**Approaching the Theoretical Limit of Diamagnetic-Induced Momentum in a Rapidly Diverging Magnetic Nozzle**

Kazunori Takahashi,[1,2,*] Christine Charles,[2] and Rod W. Boswell[2]

[1]*Department of Electrical Engineering and Computer Science, Iwate University, Morioka 020-8551, Japan*

[2]*Space Plasma, Power and Propulsion Laboratory, Research School of Physics and Engineering, The Australian National University, Canberra ACT 0200, Australia*

(Received 15 February 2013; published 8 May 2013)

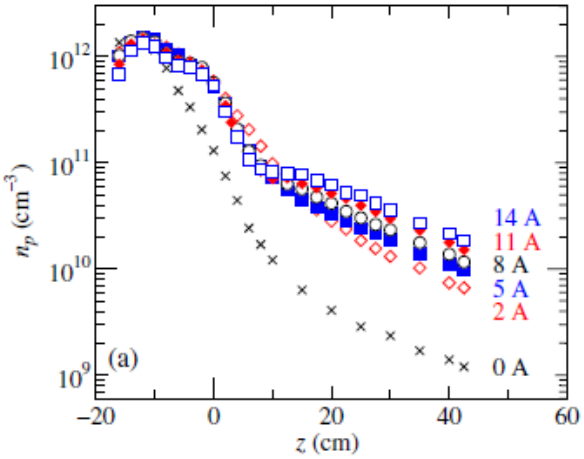


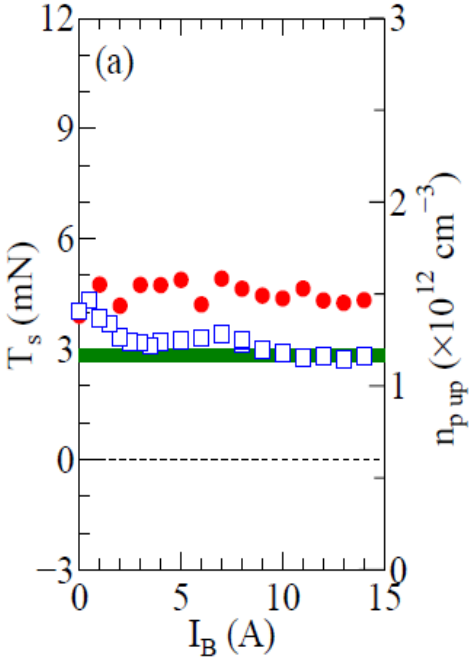


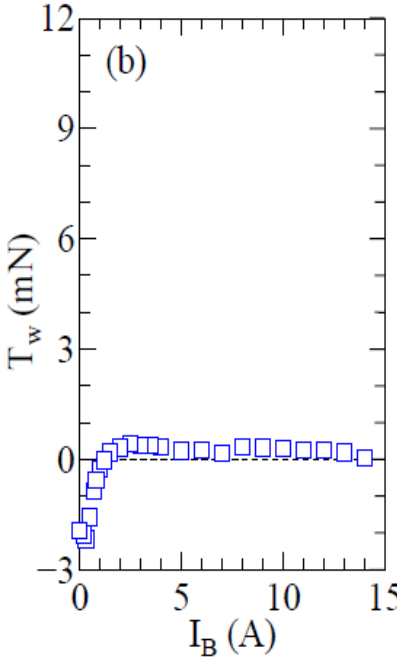


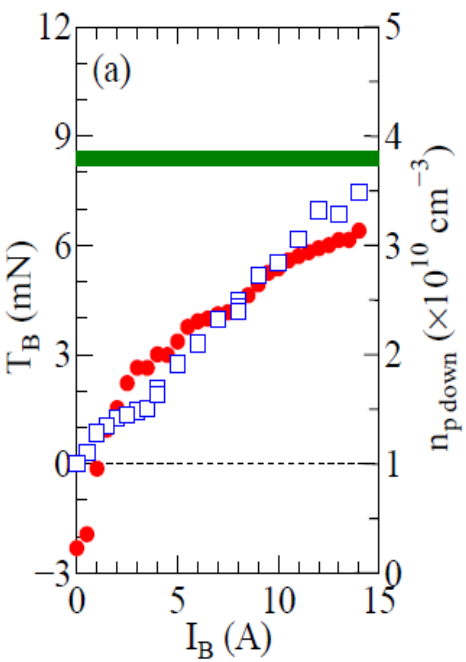


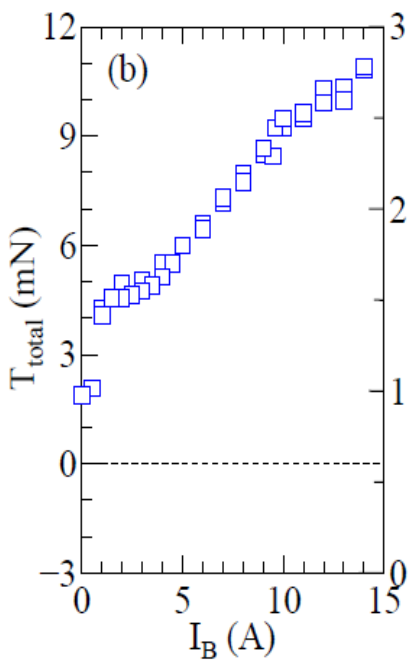

# Effect of neutral gas injection on the thrust

APPLIED PHYSICS LETTERS **109**, 194101 (2016)

## Modifications of plasma density profile and thrust by neutral injection in a helicon plasma thruster

Kazunori Takahashi,[1,a)] Yoshinori Takao,[2] and Akira Ando[1]
[1]*Department of Electrical Engineering, Tohoku University, Sendai 980-8579, Japan*
[2]*Division of Systems Research, Yokohama National University, Yokohama 240-8501, Japan*

(Received 21 September 2016; accepted 24 October 2016; published online 7 November 2016)

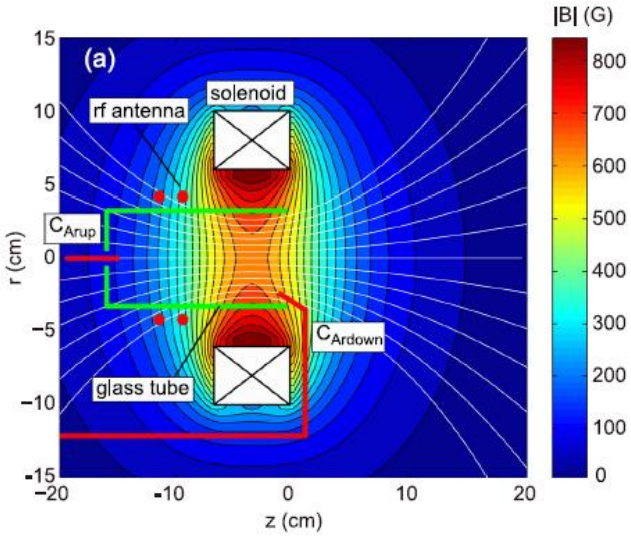


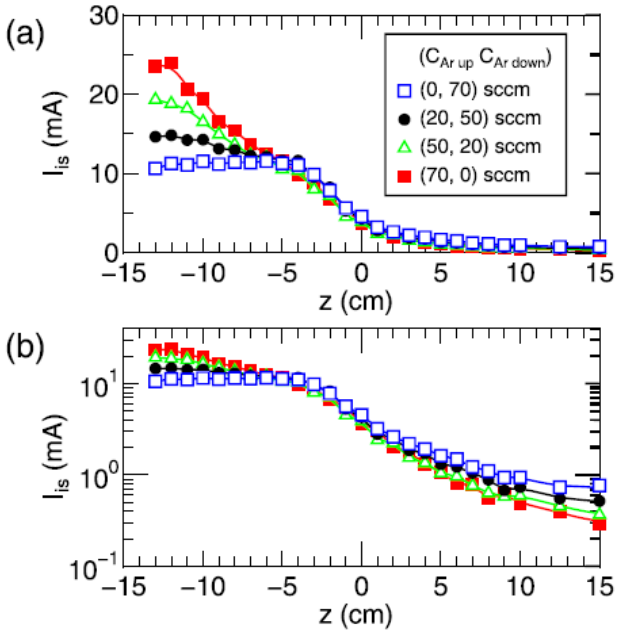


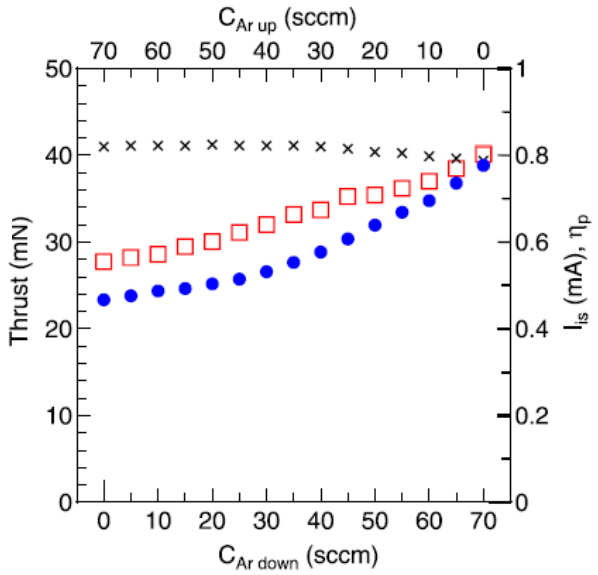


FIG. 2. The measured thrust (open squares), the rf power transfer efficiency $\eta_p$ (crosses), and the ion saturation current $I_{is}$ (filled circles) of the LP at $z = 10$ cm, as functions of the upstream ($C_{Arup}$) and downstream ($C_{Ardown}$) gas flow rates, where the top and bottom axes correspond to $C_{Arup}$ and $C_{Ardown}$, respectively.

Neutral gas injection affects the density profile and the resultant thrust generation.

# No back plate cases

Two gas injection ports for inhibiting the effect of the asymmetric neutral injection

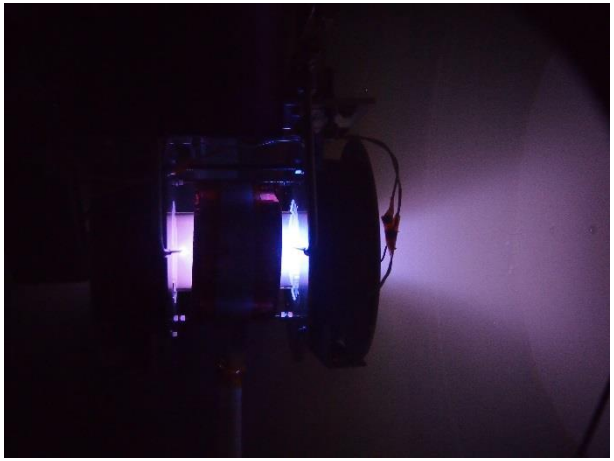

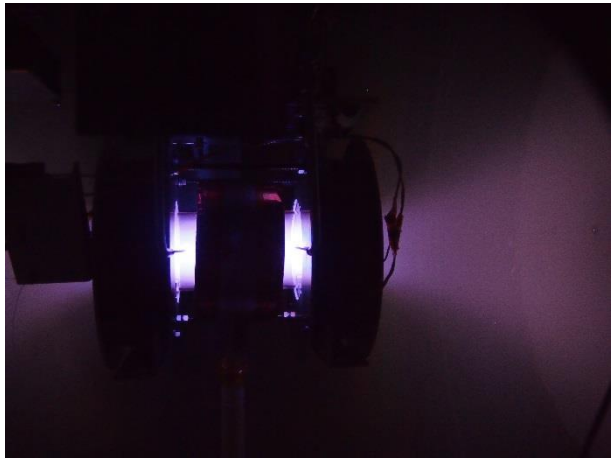

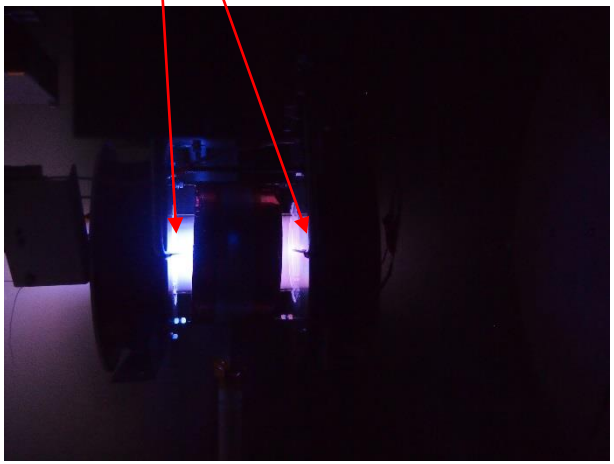

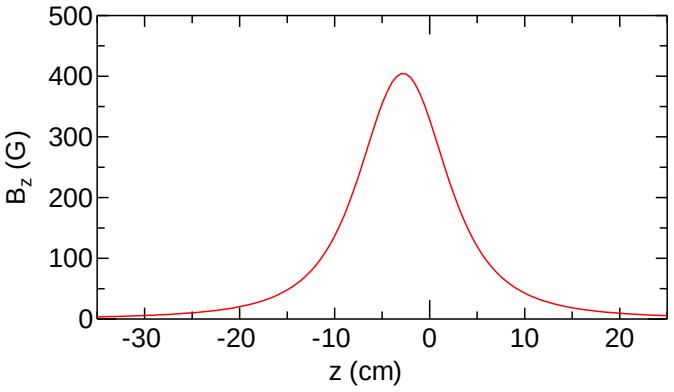


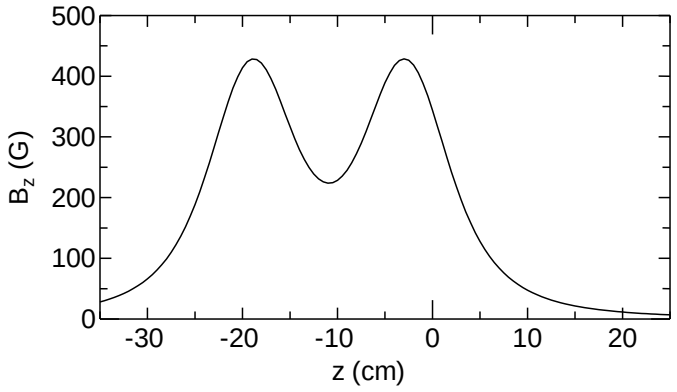


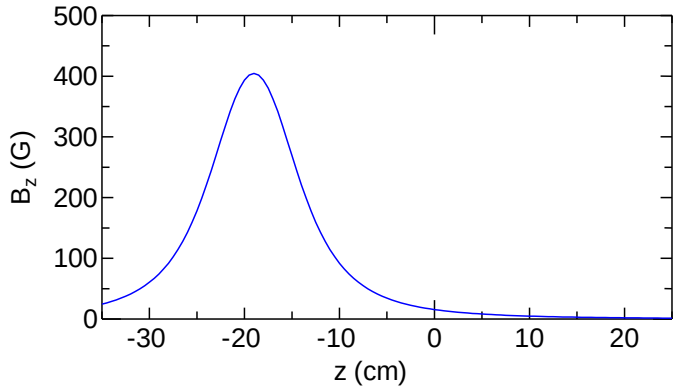

# Simultaneous measurements of the forces to the thruster and target (debris)

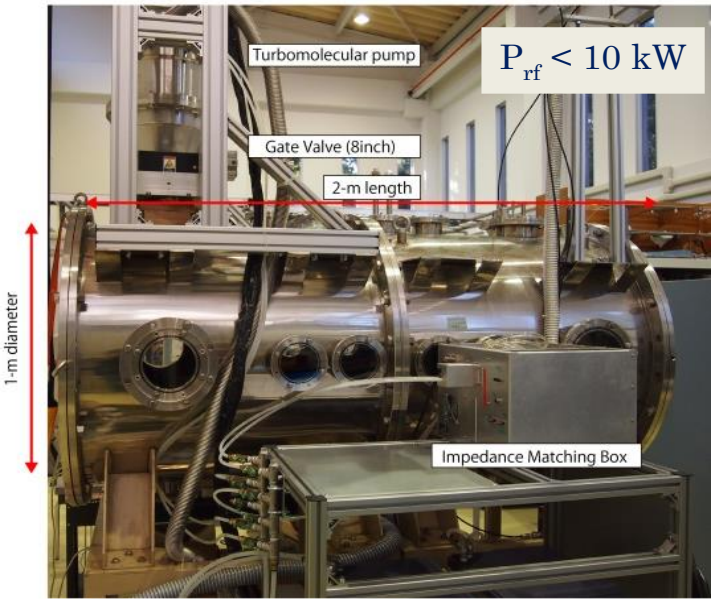


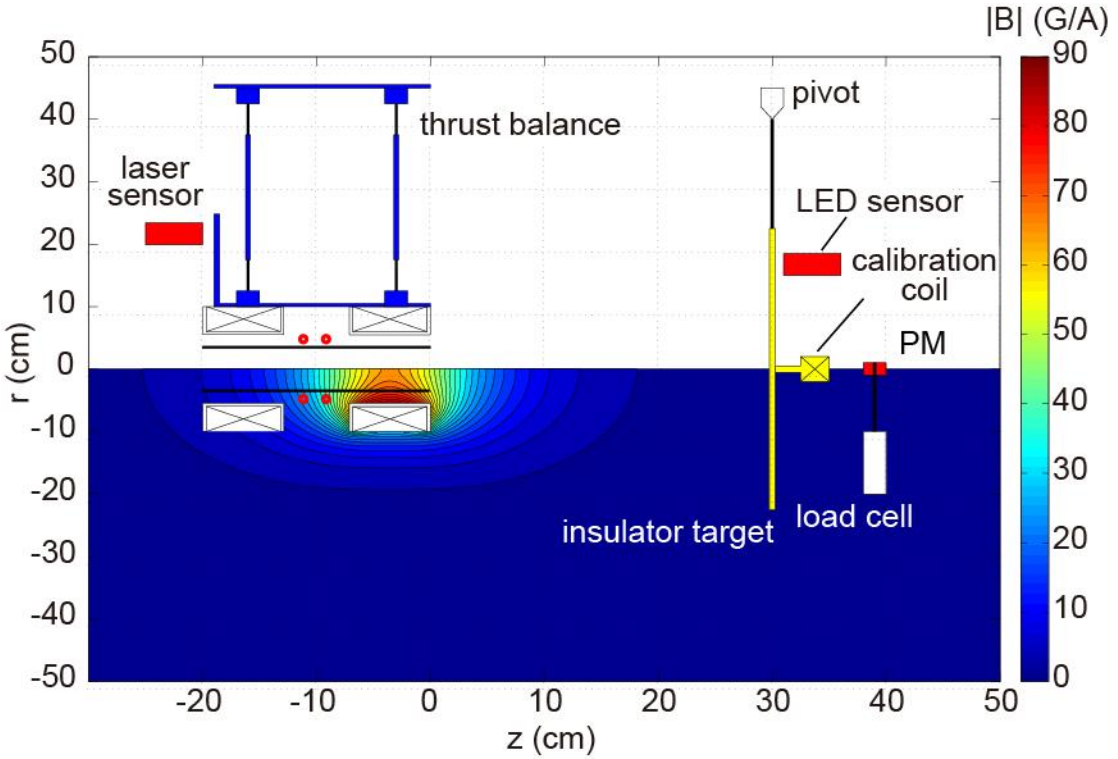

# Displacement signals

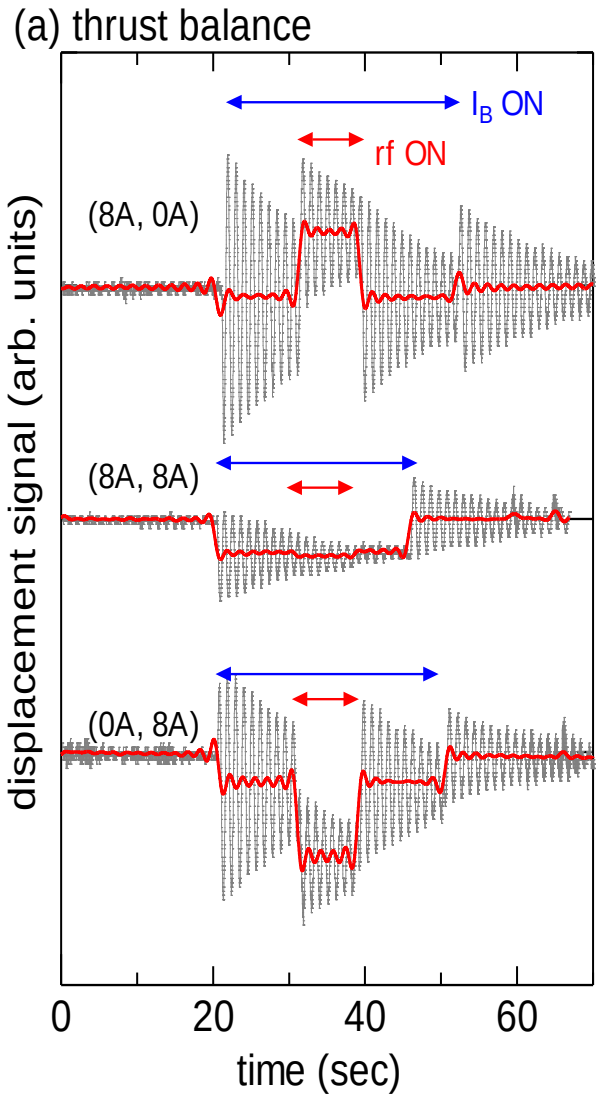


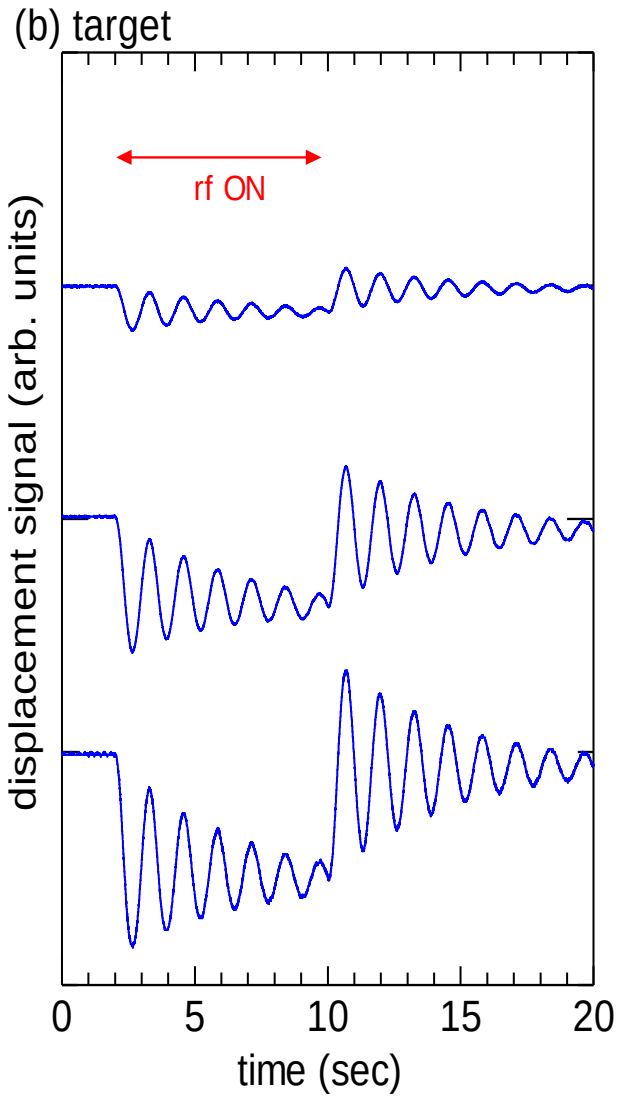


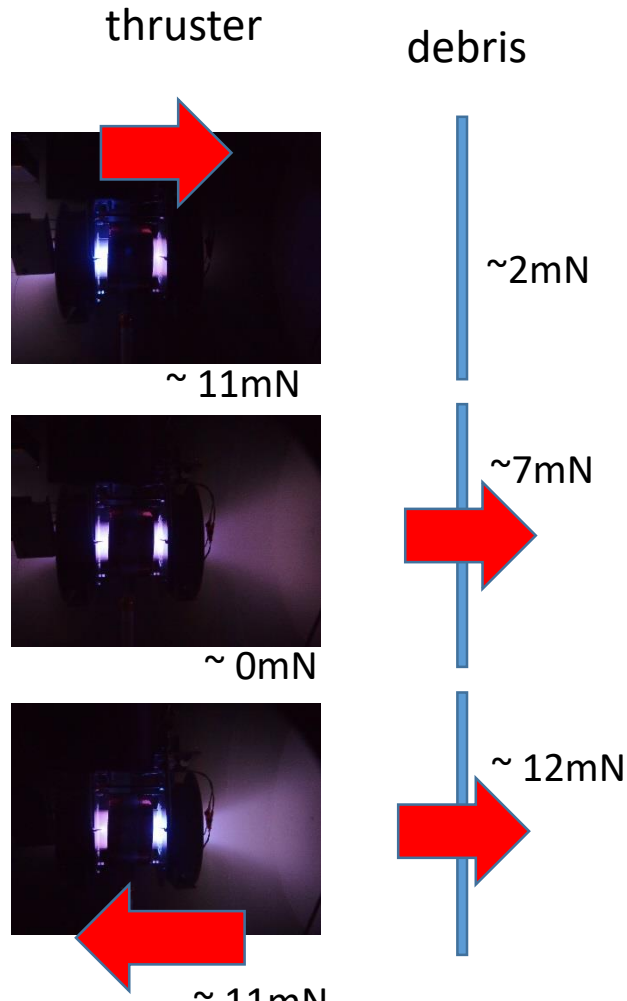

# Control by B fiend configuration

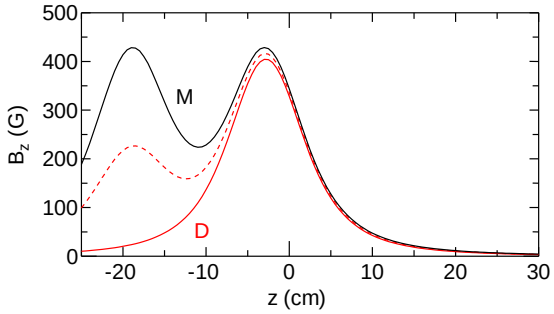


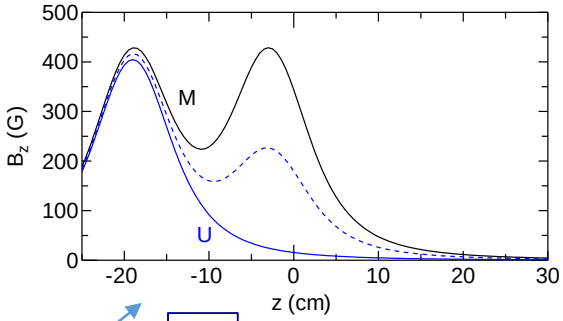


D M U

M:
zero thrust and force to the target
**Debris removal mode**

D:
Larger thrust accelerating the spacecraft
**Acceleration mode**

U:
Large thrust decelerating the spacecraft
**Deceleration mode**

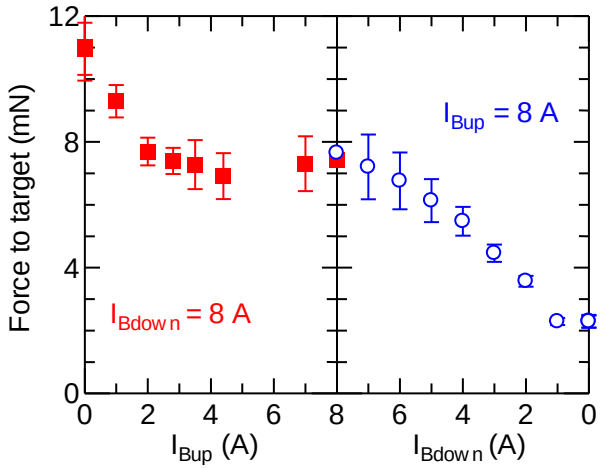


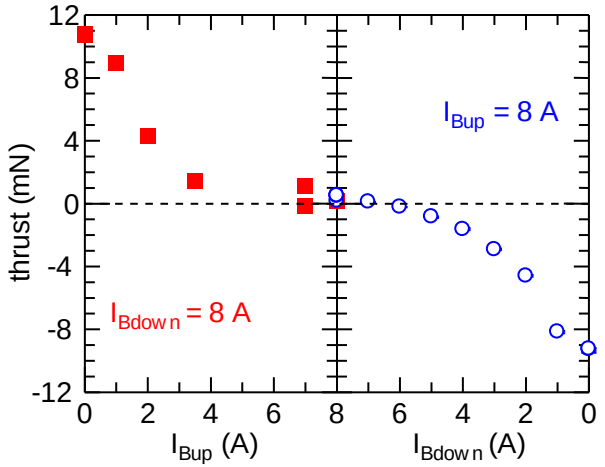


C:\KazunoriTakahashi\DataDrive\Experiments_MegaHPT\20170626MegaHPTKazu_Debris\Momentum_IBupIBdown_1kW50sccm50sccm\Thrust_IBupIBdown.ngp

# Density measured at 25 cm upstream and downstream of the thruster exits

Thruster center is z = -10.9 cm.

The measurements are performed at z = -35.9 cm and 14.1 cm.

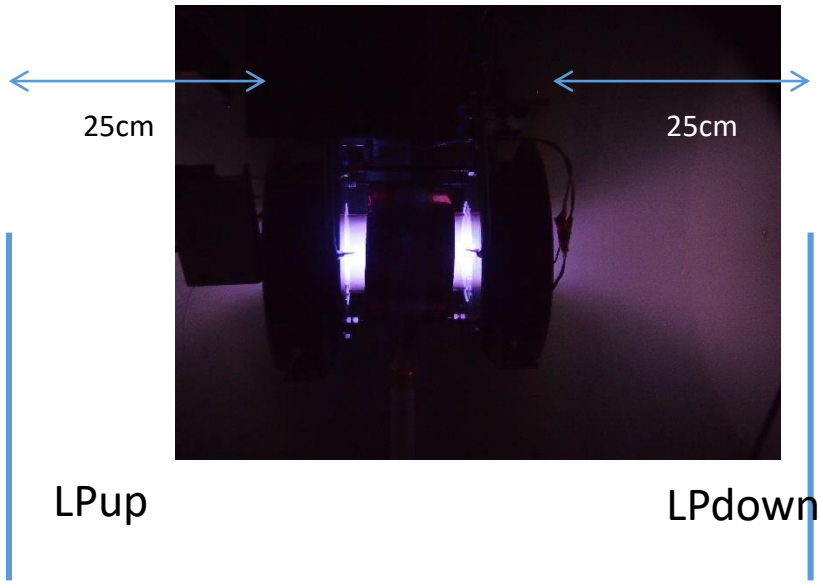


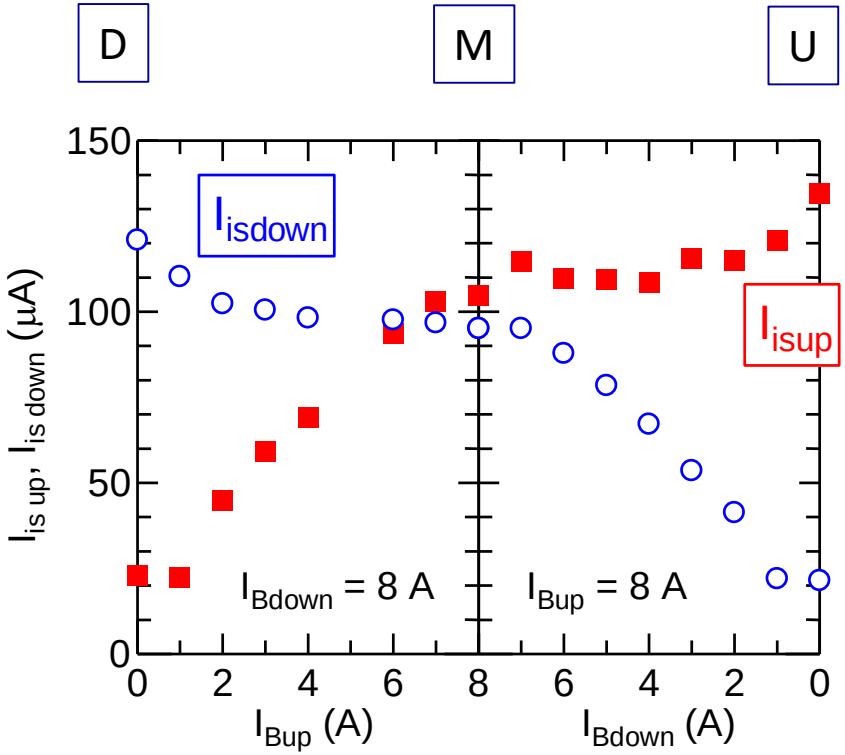


C:\KazunoriTakahashi\DataDrive\Experiments_MegaHPT\20170623MegaHPTKazu_Debris\Iisupdown_IB_1kWCup50Cdown50.ngp

# Axial density profiles

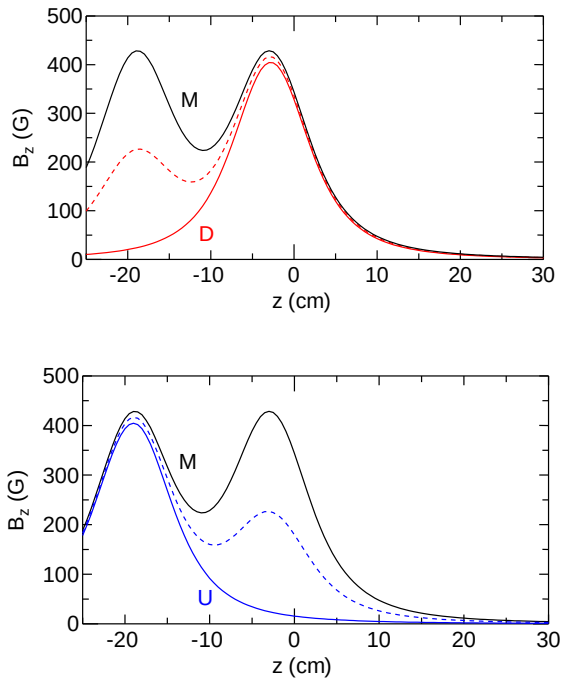


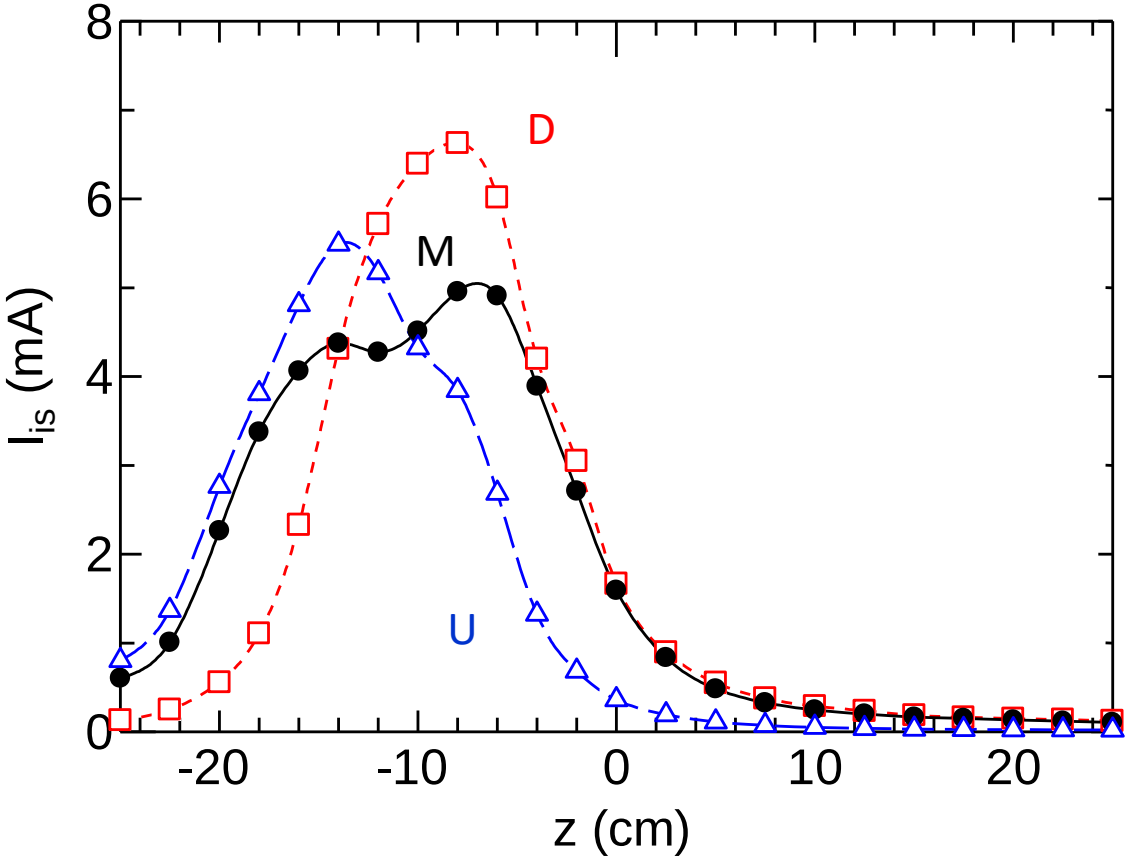


The density profile modified by the magnetic field configuration (perhaps ionization profile or the inhibition of the loss to the wall by separating the plasma from the wall) seems to dominate the momentum exhausted into the upstream and downstream direction.

C:\KazunoriTakahashi\DataDrive\Experiments_MegaHPT\20170623MegaHPTKazu_Debris\Iisd own_zdown_Bconfig.ngp

# Control by gas injection

C:\KazunoriTakahashi\DataDrive\Experiments_MegaHPT\20170626MegaHPTKazu_Debris\Momentum_CArRatio_1kW8A8A\Thrust_CupCdown.ngp

**Debris removal mode**

**Acceleration mode**

**Deceleration mode**

$I_{Bup} = I_{Bdown} = 8A$

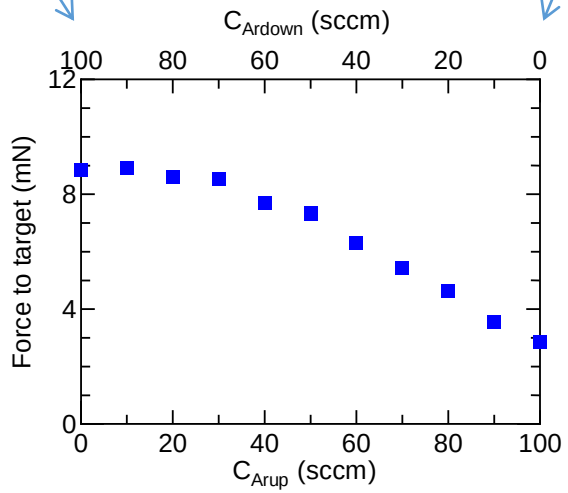


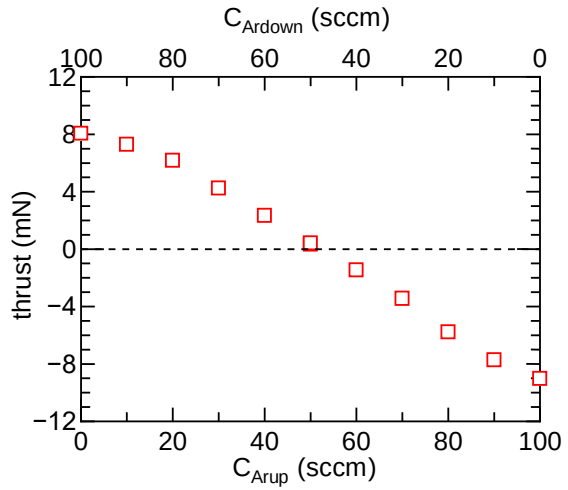


The debris removal, acceleration, and deceleration modes can be switched by the gas injection.
This is not due to the cold gas thrust, but the plasma density modification by the neutral.

Actually, the improved thrust has been observed by the previous experiments. (Takahashi APL 2016b)

Takao is now working on the DSMC-PIC simulations with a magnetic field, we can ask to Takao to simulate the present experiments if needed.

# Density measured at 25 cm upstream and downstream of the thruster exits

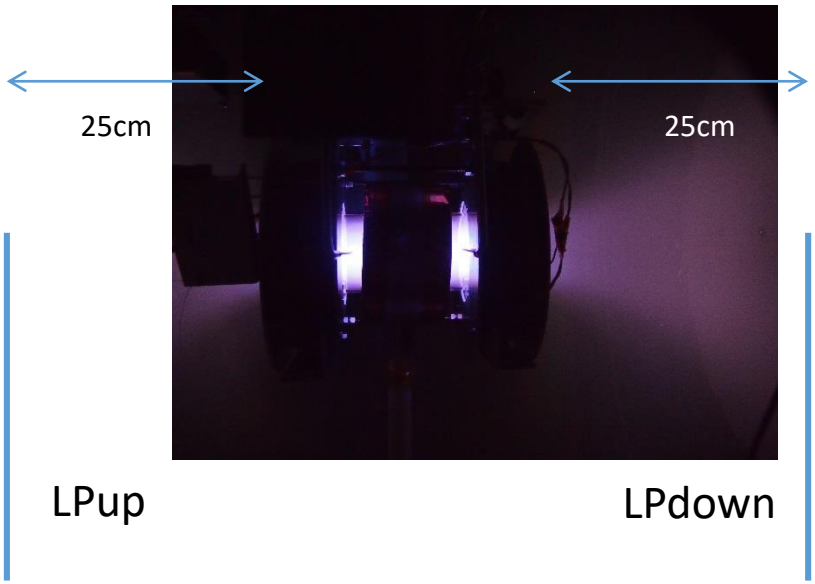


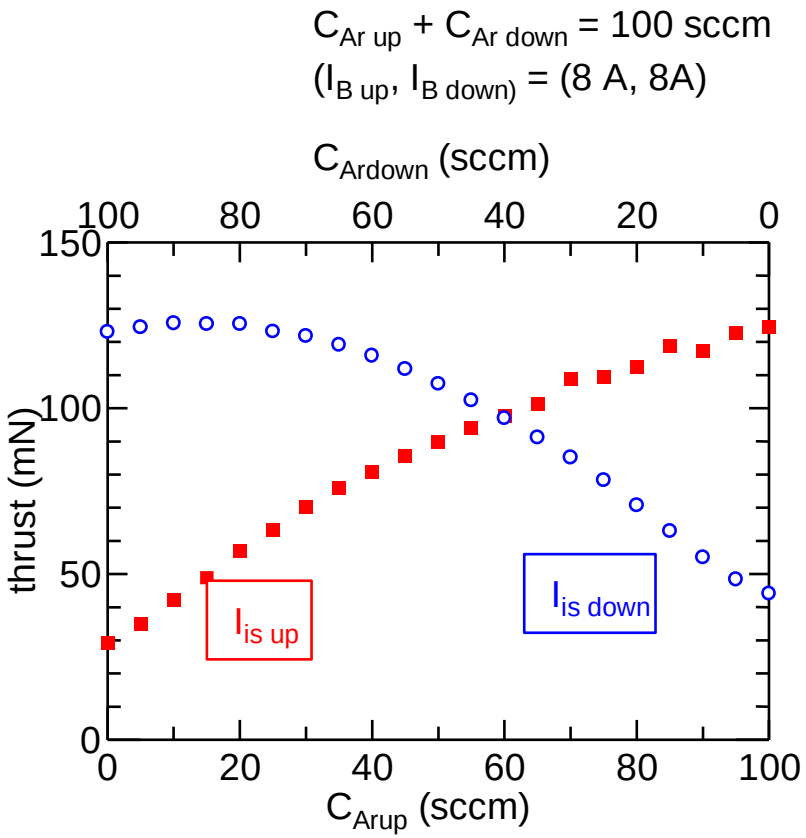


C:\KazunoriTakahashi\DataDrive\Experiments_MegaHPT\20170623MegaHPTKazu_Debris\Iisupdown_CupCdown.ngp

C:\KazunoriTakahashi\DataDrive\Experiments_MegaHPT\20170623MegaHPTKazu_Debris\Iisdown_zdown_CArRatio.ngp

# Axial density profiles

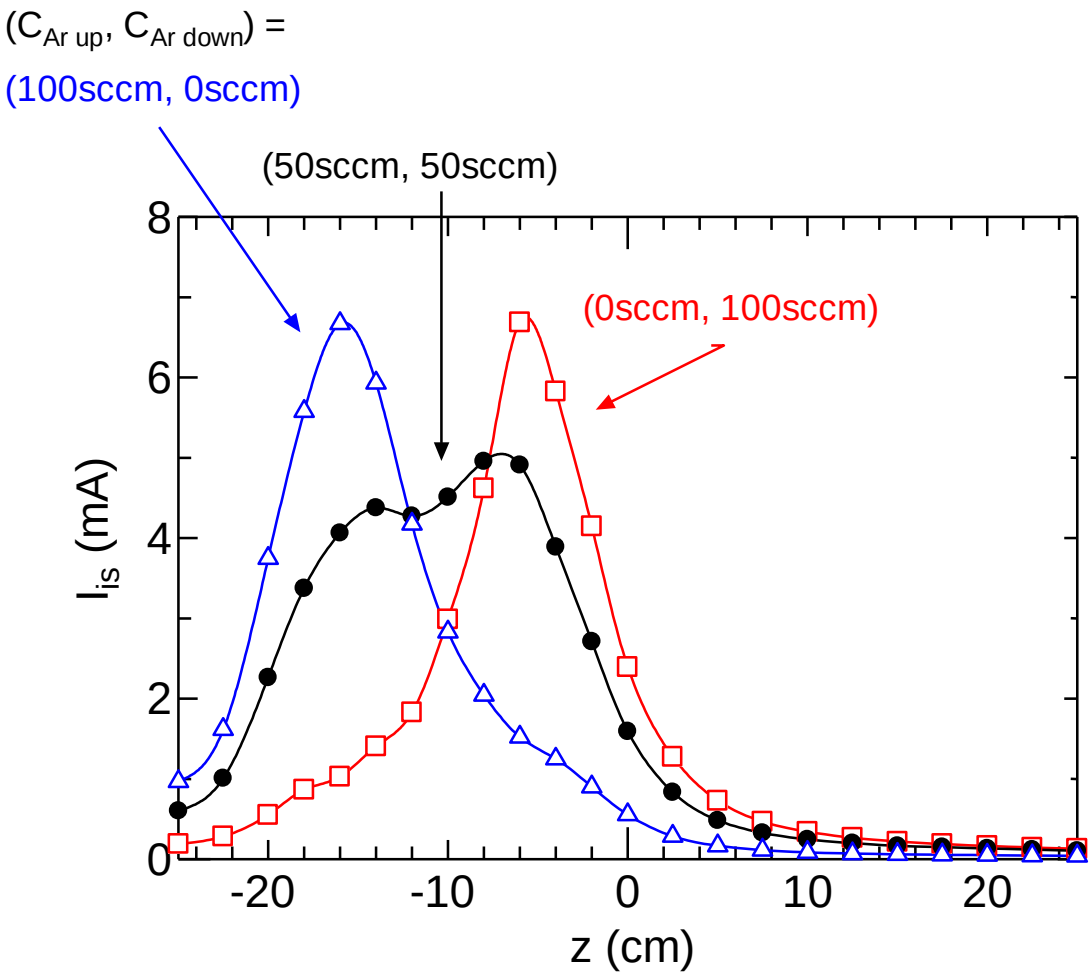


The local ionization seems to be one of the reasons why the density upstream and downstream of the exits are controlled by the gas injection.

# Conclusion

The upstream and downstream plasma flows exhausted from the helicon plasma thruster is successfully controlled by the magnetic field configuration.

The simultaneous measurement of the forces to the thruster and the target demonstrates the concept of the space debris removal by one electric propulsion device.

Furthermore, the thruster can be operated at ‘space debris removal mode’, ‘acceleration mode’, and ‘deceleration mode’ for the different magnetic field configurations, i.e., all the operation modes can be performed by the one electric propulsion device.

# Electrostatic acceleration and energy transfer from electrons to ions

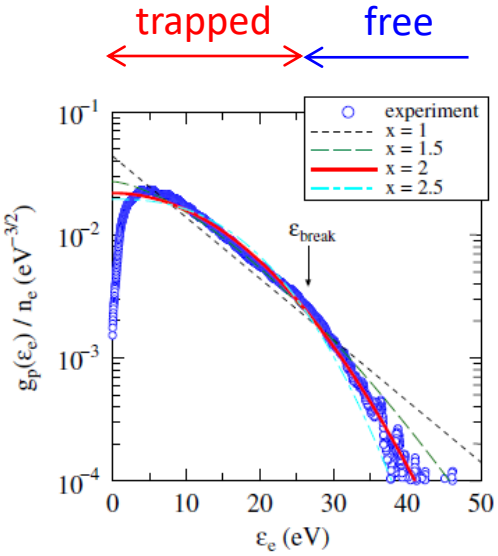


PHYSICS OF PLASMAS VOLUME 11, NUMBER 4 APRIL 2004

**Laboratory evidence of a supersonic ion beam generated by a current-free "helicon" double-layer**

C. Charles[a] and R. W. Boswell
*Plasma Research Laboratory, Research School of Physical Sciences and Engineering, The Australian National University, Acton, ACT 0200, Australia*

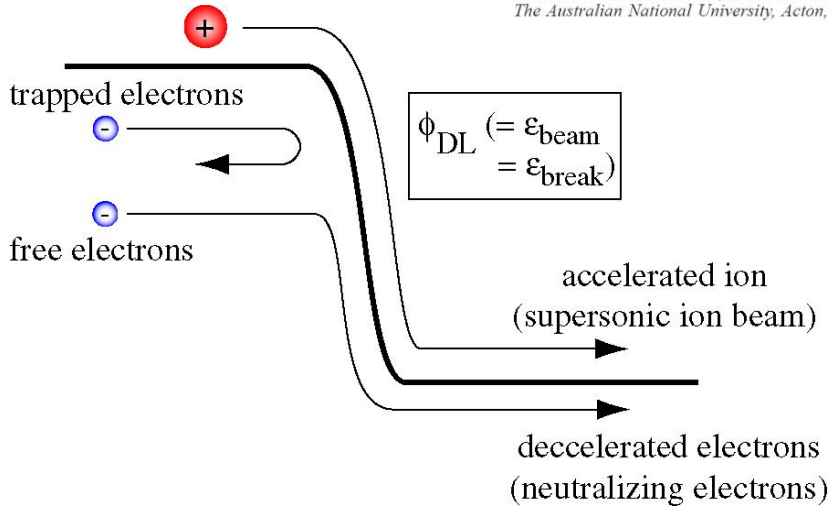


PRL **107,** 035002 (2011) PHYSICAL REVIEW LETTERS week ending 15 JULY 2011

**Electron Energy Distribution of a Current-Free Double Layer: Druyvesteyn Theory and Experiments**

Kazunori Takahashi,[1,2,*] Christine Charles,[1] Rod W. Boswell,[1] and Tamiya Fujiwara[2]
[1]*Space Plasma, Power and Propulsion Group, Research School of Physics and Engineering, The Australian National University, Canberra ACT 0200, Australia*
[2]*Department of Electrical Engineering and Computer Science, Iwate University, Morioka 020-8551, Japan*
(Received 7 April 2011; published 11 July 2011)

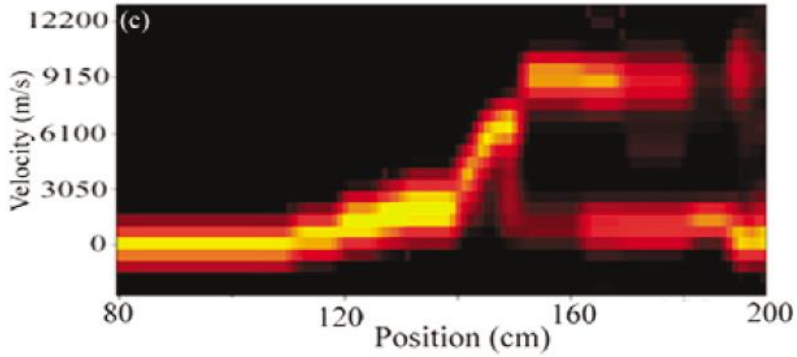

# Axial momentum lost to the radial wall

PRL 114, 195001 (2015) PHYSICAL REVIEW LETTERS week ending 15 MAY 2015

**Axial Momentum Lost to a Lateral Wall of a Helicon Plasma Source**

Kazunori Takahashi,* Aiki Chiba, Atsushi Komuro, and Akira Ando
*Department of Electrical Engineering, Tohoku University, Sendai 980-8579, Japan*
(Received 15 January 2015; published 12 May 2015)

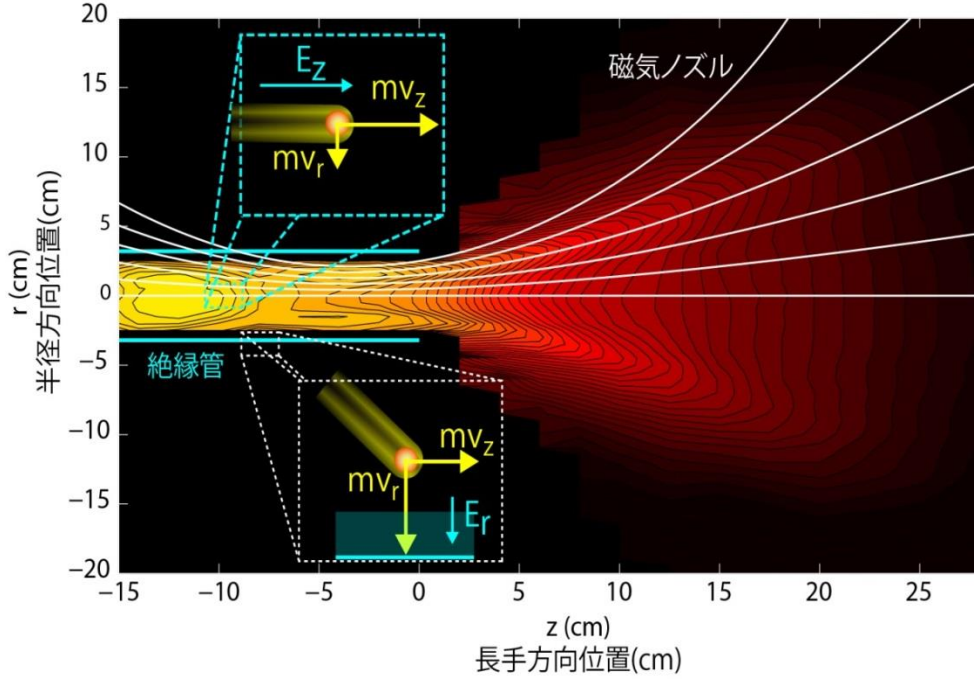


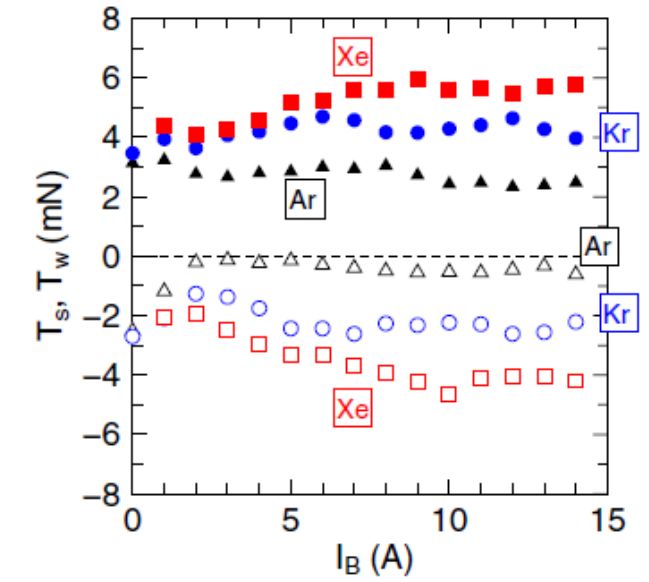


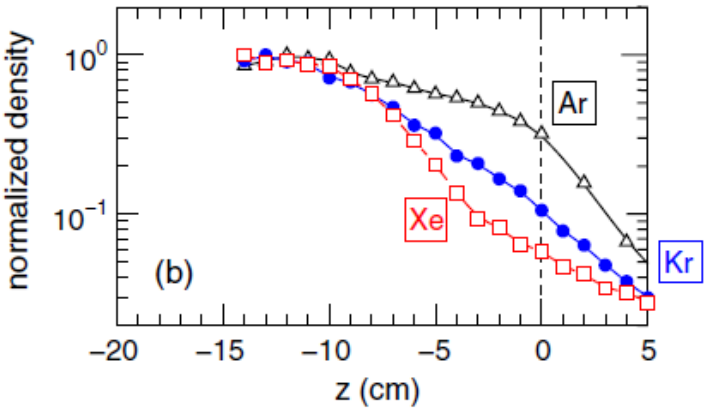


Density profile shifted to the upstream side seems to be connected to the loss term.
Such profile seems to be due to a neutral depletion effect.

# Laboratory Observation of a Plasma-Flow-State Transition from Diverging to Stretching a Magnetic Nozzle

Kazunori Takahashi* and Akira Ando
*Department of Electrical Engineering, Tohoku University, Sendai 980-8579, Japan*
(Received 20 February 2017; revised manuscript received 18 April 2017; published 2 June 2017)

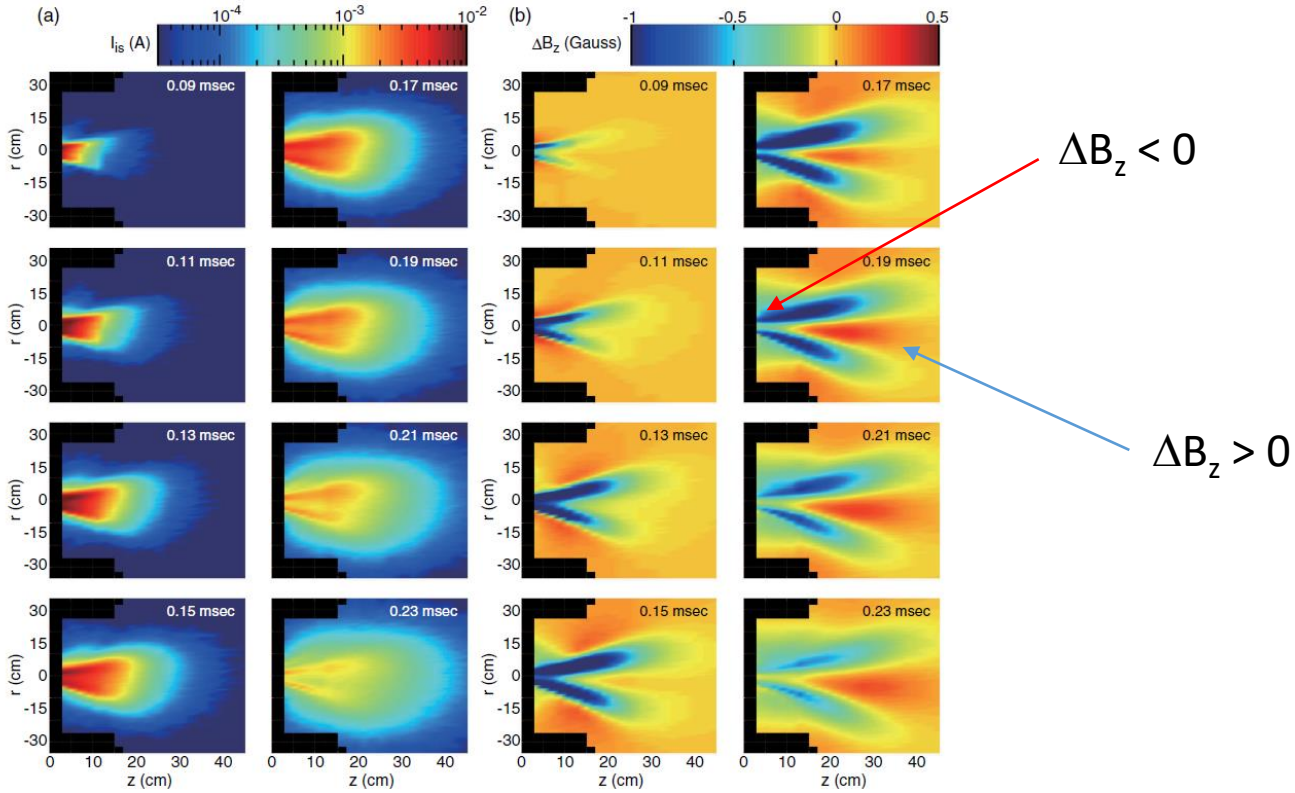


FIG. 2. Spatiotemporal evolution of (a) $I_{is}$ and (b) $\Delta B_z$, taken for $I_B = 4.5$ A and $P_{rf} = 5$ kW. The rf power is triggered at $t = 0$ and the signals are averaged over 16 shots, where the measurements are performed at ~1200 points (~20 points along $z$ and ~60 points along $r$). A movie can also be found as Supplemental Material [29].

# Physical picture of the data

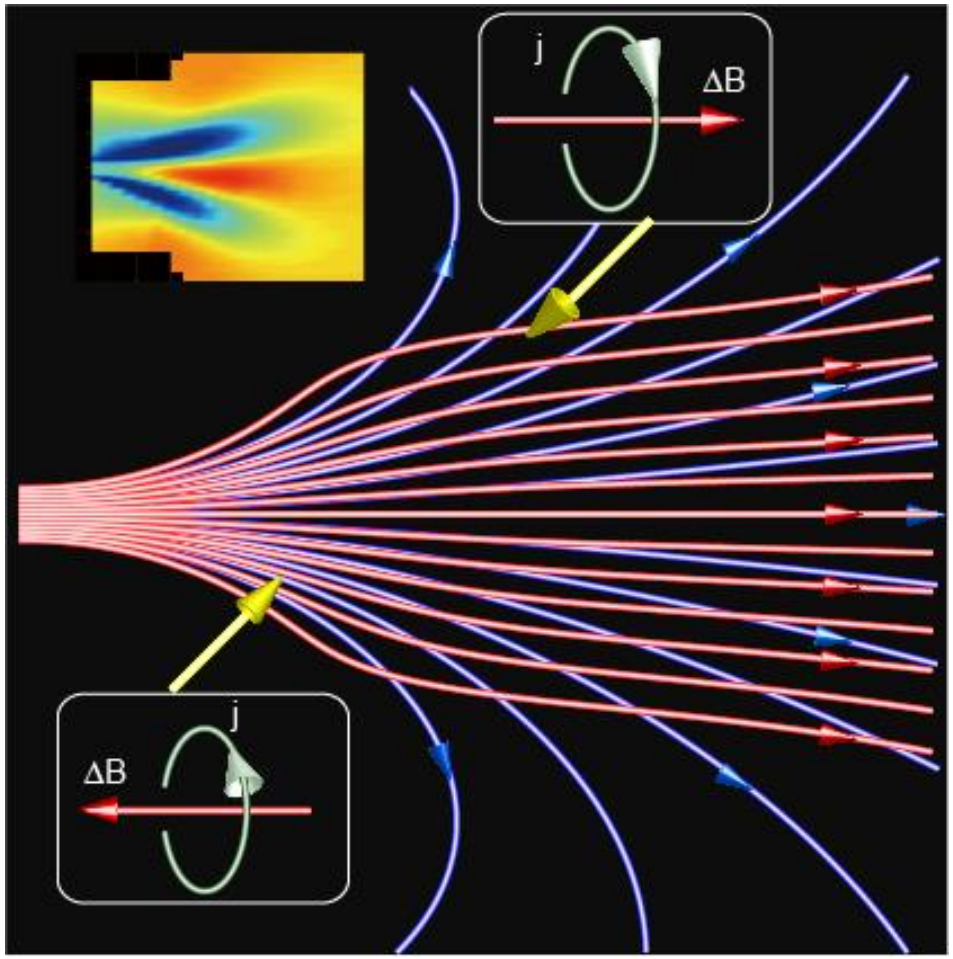


PHYS ORG:

**On the road to creating an electrodeless spacecraft propulsion engine**

# Transition condition analysis

V = Mi*Cs ~ 3.5 km/s

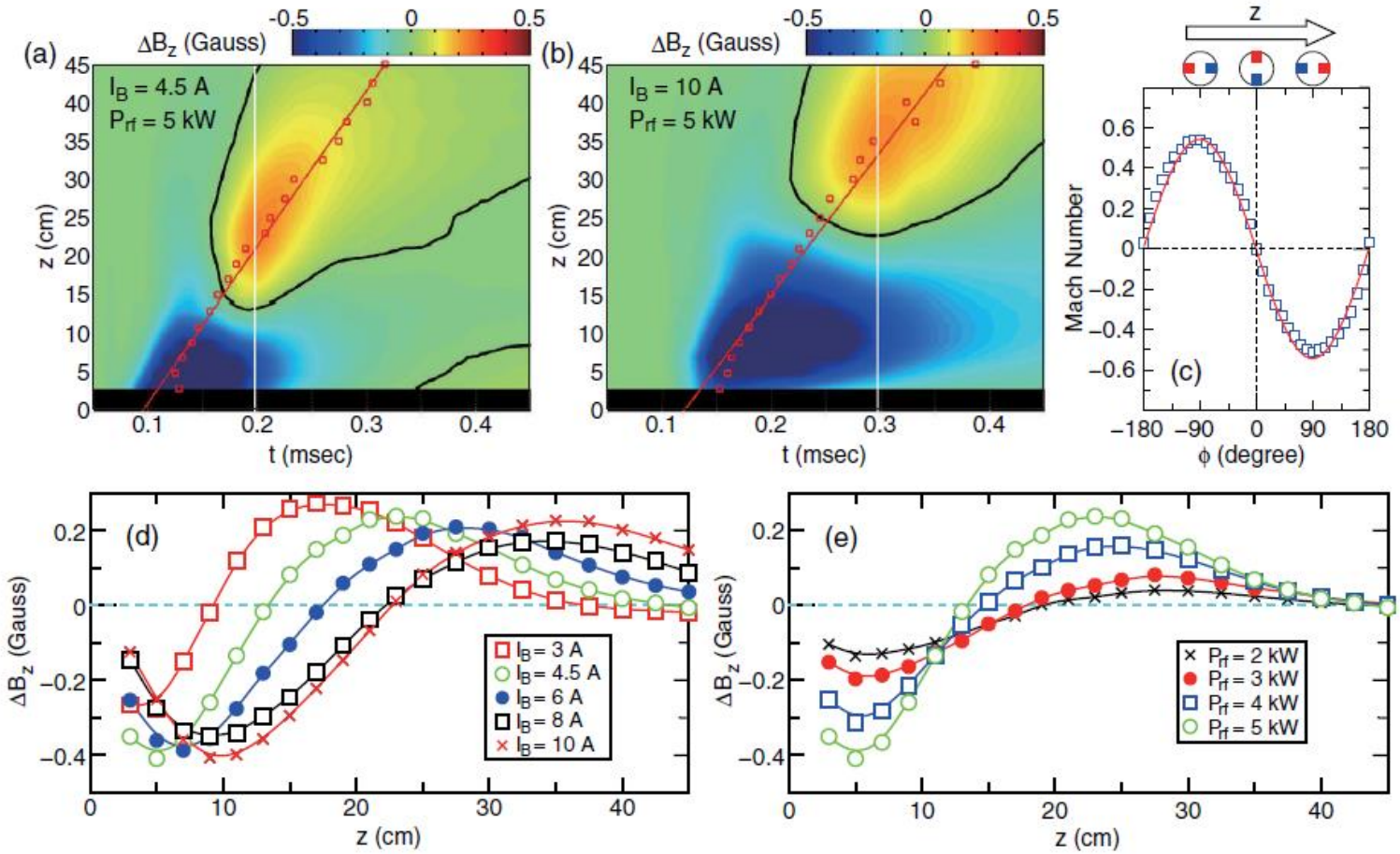


FIG. 3. (a),(b) Temporal evolutions of the axial profile of $\Delta B_z$ on axis for $I_B = 4.5$ and 10 A. Open squares are the times giving the temporal density peak as a function of $z$, and the fitted lines correspond to the propagation velocity of the density peak. White solid lines show the time giving the maximum $\Delta B_z$. Black solid lines correspond to the contour lines of $\Delta B_z = 0$ implying the diverging-to-stretching transition. (c) Ion Mach number measured by the MP at $z = 20$ cm as a function of the rotational angle $\phi$ of the probe shaft together with the fitted sin function. (d),(e) Axial profiles of $\Delta B_z$ as functions of $I_B$ and $P_{\mathrm{rf}}$, where the data at the times giving the maximum $\Delta B_z$ [white solid lines in Figs. 3(a) and 3(b)] are plotted.

Takahashi and Ando, PRL2017

# What parameter decides the transition?

Many people believe that the stretch occurs for the super Alfvénic flow ($M_A = v/v_A > 1$)

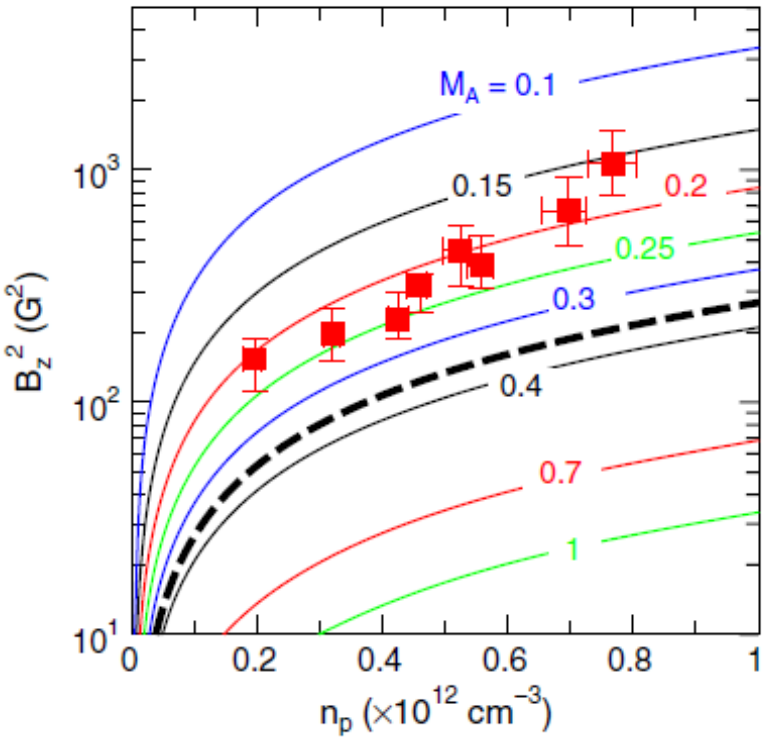


FIG. 4. Measured plasma density $n_p$ and the square of the applied magnetic field strength $B_z$ at the transition positions. The solid lines and the bold dashed line correspond to Eq. (1) for various values of the Alfvén Mach number $M_A$ and Eq. (3), respectively, where the measured values of $v = 2$ km/s and $T_e = 5$ eV are used for the calculation.

The experiment shows that the transition occurs at the lower Alfvén Mach Number than people thought.

Takahashi and Ando, PRL2017

# Transition model in an ideal MHD approximation (1)

Magnetic pressure force

Inertia term

$$\rho(\mathbf{v}\cdot\nabla)\mathbf{v} = -\nabla p - \frac{\nabla B^2}{2\mu} + \frac{(\mathbf{B}\cdot\nabla)\mathbf{B}}{\mu},$$

Pressure force

Magnetic tension

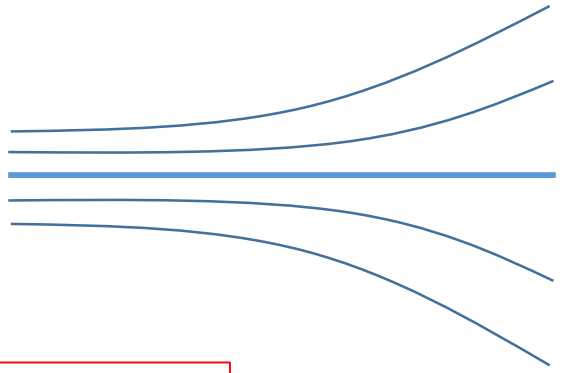

**Upstream limit**

1- Zero velocity (v ~ 0)

2- Straight axial magnetic field
(negligible tension term)

$$\nabla\left(p + \frac{B^2}{2\mu}\right) = 0,$$

hence $$p + \frac{B^2}{2\mu} = \frac{B_{vac}^2}{2\mu},$$

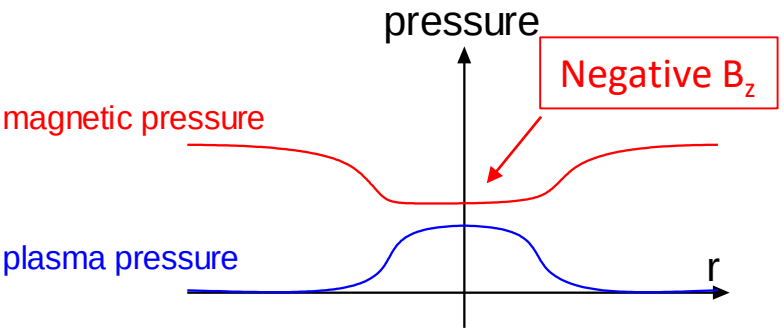


**Downstream limit**

1- low plasma pressure (p ~ 0)

2- low magnetic field
(negligible magnetic pressure)

$$\rho(\mathbf{v}\cdot\nabla)\mathbf{v} = \frac{(\mathbf{B}\cdot\nabla)\mathbf{B}}{\mu}.$$

$$\left|\frac{\rho v^2}{L}\right| \simeq \left|-\frac{B^2}{\mu L}\right|$$

$$v^2 \sim V_A^2 = \frac{(B_{vac}+\Delta B)^2}{mn\mu}$$

For $v > V_{Avac} = \frac{B_{vac}}{\sqrt{mn\mu}}$

ΔB should be positive to maintain the equilibrium.

# Transition model in an ideal MHD approximation (2)

Intermediate condition

Takahashi and Ando, PRL2017

$$\rho(\mathbf{v}\cdot\nabla)\mathbf{v} = -\nabla p - \frac{\nabla B^2}{2\mu} + \frac{(\mathbf{B}\cdot\nabla)\mathbf{B}}{\mu},$$

Dimension analysis
(∇ → 1/L for velocity
and -1/L for the decreasing B and p)

$$\left|\frac{\rho v^2}{L}\right| \simeq \left|\frac{p_e}{L} + \frac{B^2}{2\mu L} - \frac{B^2}{\mu L}\right|,$$

$$= \left|\frac{nk_B T_e}{L} - \frac{B^2}{2\mu L}\right|.$$

$$v^2 \sim \frac{1}{2}V_A^2 - C_s^2 = \frac{1}{2}\frac{(B_{vac}+\Delta B)^2}{mn\mu} - C_s^2$$

$$\text{For } v^2 > \frac{1}{2}V_{Avac}^2 - C_s^2 = \frac{1}{2}\frac{B_{vac}^2}{mn\mu} - C_s^2,$$

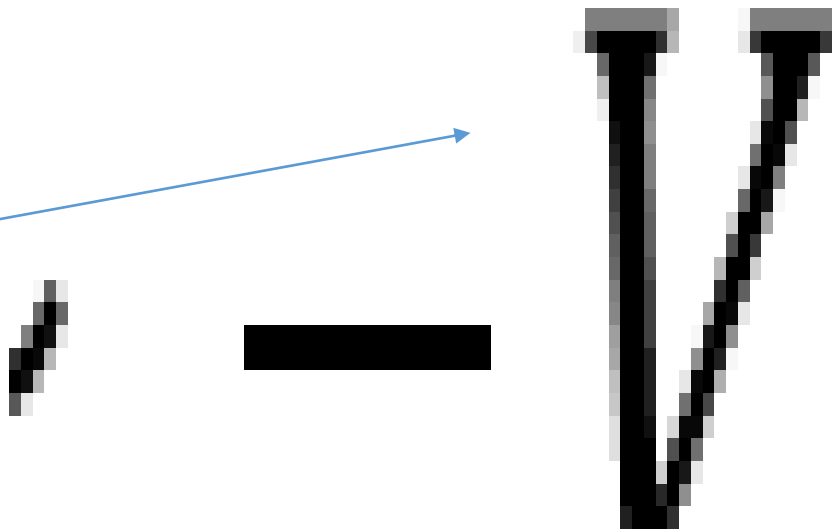

ΔB should be positive to maintain the equilibrium.